UDC 550.34. + 550.348 + 550.348.098.4

Valērijs ŅIKUĻINS[1], Dmytro MALYTSKYY[2]

[1] SIA Geo Consultants, Olivu iela, 9, Riga, LV-1004, Latvia, e-mail: seismolat@gmail.com, https://orcid.org/0000-0003-4489-8708

[2] Carpathian Branch of Subbotin Institute of Geophysics, National Academy of Sciences of Ukraine, e-mail: dmalytskyy@gmail.com, https://orcid.org/0000-0002-9156-739X

https://doi.org/10.23939/jgd2024.02.016

MODEL OF TECTONIC STRESS IN THE EASTERN BALTIC REGION

The parameters and mechanisms of the source of modern earthquakes in the Eastern Baltic region are systematized. The predominant types of focal mechanisms of continental earthquakes are ***strike-slip*** and ***reverse***. A generalized map of the orientation of maximum horizontal stresses in the East Baltic region and adjacent territories has been created. To create this map, we utilized the World Stress Map database and added the directions of maximum horizontal stresses in Estonia. The direction of maximum horizontal stresses changes from north (Estonia) to south (Kaliningrad region of Russian Federation) from 102º–114º to 157º–166º. The study investigated how the deep geological structure and gravitational forces in different parts of the earth's crust affect the direction of maximum horizontal stresses. It was observed that the direction of maximum horizontal stress changed when crossing only one of a deep tectonic fault. The direction of maximum horizontal stress showed the high correlation values with the gravitational effect of the sedimentary cover (negative correlation), the averaged difference gravitational field, and the gravitational effect of the crustal layer up to the *Conrad* boundary.

Keywords: earthquake focal mechanism, seismic moment tensor, earthquake source parameters, principal stresses, maximum horizontal stress, Eastern Baltic region, World Stress Map.

Introduction

Tectonic stress is the most important physical quantity that controls the occurrence of earthquakes. Knowledge of the stressed state of the earth's crust is essential for understanding geodynamic processes, reactivation of tectonic faults near energy facilities, disposal of hazardous environmental waste, including radioactive waste, and underground hydrocarbon storage facilities. Considering existing stressses is necessary to minimize the consequences of changes in the regime of man-made loads (changing the water level in a reservoir, unloading or pumping gas into an underground reservoir, etc.). Regional stresses are of particular interest when it comes to quantifying tectonic deformation near faults and the associated earthquake hazard [Hergert and Heidbach, 2011].

On the territory of the East Baltic Region (EBR) there are nuclear power facilities (Belarusian and Leningrad nuclear power plants), hydropower facilities (*Plavinu* and other hydroelectric power stations), hazardous waste storage facilities, including radioactive waste (*Ignalina*, Lithuania; *Baldone*, Latvia), underground hydrocarbon storage facilities (*Incukalns* underground gas storage, Latvia). The safety of such objects requires knowledge of geodynamic conditions, including the direction and magnitude of tectonic stresses. Tectonic stresses are an important indicator for assessing processes in the earth's crust, including fracturing, the possibility of earthquakes, and tectonic creep. The main parameters of tectonic stress are the orientation (vector) and magnitude (scalar) of the maximum horizontal tectonic stress $S_{H\max}$.

These studies are devoted to the analysis of the orientation of $S_{H\max}$ in the East Baltic region (EBR), which includes Estonia, Latvia, Lithuania, the Kaliningrad region of the Russian Federation and the adjacent Baltic Sea. The initial information about $S_{H\max}$ is based on World Stress Map (WSM) data. Various methods are used to estimate $S_{H\max}$, but the main method is based on solving the focal mechanism of earthquakes.

The EBR is located far from the boundaries of tectonic plates and is characterized by low seismic activity. Seismic activity in the EBR is heterogeneous. The relatively high seismic activity is observed in Estonia, and the lowest in Lithuania. The strongest EBR earthquakes occurred in the Kaliningrad region of the Russian Federation in 2004 [Gregersen et al., 2007]. Before the beginning of the instrumental period (the 1960s), several historical earthquakes occurred in the EBR. Information about them is mainly contained in the works of B. Doss (1910), A. Nikonov and H. Sildvee (1991), A. Boborykin [Avotinya et al., 1988; Boborykin et al., 1993]. These earthquakes were not recorded instrumentally. For them, the shaking intensity at the epicenter is known, and then the hypocenter magnitude and depth are

indirectly estimated. During the instrumental period, starting from the mid-1960s, relatively strong earthquakes occurred in Estonia (Osmussaar, M = 4.7) in 1976 and the Kaliningrad region of the Russian Federation (M = 5.0 and 5.2) in 2004. Several weaker earthquakes have been recorded in Estonia from 1980 to 2018. The number of earthquakes for which solutions of focal mechanisms in EBR were obtained is limited. All earthquake source solutions for the instrumental observation period in the EBR were added to the WSM database to calculate the S_{Hmax} orientation model.

Methods and materials

Data on $S_{H\max}$ are distributed unevenly in the earth's crust. In regions with high seismic activity, such as the Mid-Atlantic ridge between Greenland and Scandinavia, there are more earthquakes, whereas in areas with low seismic activity (EBR), their number is limited.

The azimuth and magnitude of the maximum horizontal tectonic stress $S_{H\max}$ can be determined by various methods. The World Stress Map (WSM) database [Heidbach et al., 2016; Heidbach et al., 2018] was used to map $S_{H\max}$. Information about $S_{H\max}$ contained in the WSM database was obtained based on 8 methods (Focal Mechanisms Single (FMS), Focal Mechanisms Inversion (FMF), Borehole Breakouts (BO, BOC, BOT), Drilling Induced Tensile fracture (DIF), Hydraulic Fracturing (HF, HFG, HFM, HFP), Geological (GFI, GFM, GFS, GVA), Overcoring (OC), Other (BS, FMA, PC, SWB, SWL, SWS)). However, for the study area, $S_{H\max}$ directions are obtained mainly using four methods: Earthquake Focal Mechanism (Scandinavia and Eastern Baltic region), Hydraulic Fracturing (southern Sweden and Finland) and Overcoring (southern Sweden and Finland), Borehole Breakouts (water area and coast of northern Poland). The predominant amount of $S_{H\max}$ was obtained based on the Earthquake Focal Mechanisms method [Heidbach et al., 2018].

Each data set is assigned a certain accuracy class from A to E. The accuracy class determines the deviation of the azimuth $S_{H\max}$ from its average value. Class A corresponds to a deviation of ± 15º, Class B: ±20º, Class C: ±25º, Class D: ±40º, and Class E corresponds to a deviation > ±40º. The main contribution to the assessment of $S_{H\max}$ in the WSM 2016 database comes from methods based on solving the earthquake focal mechanism. For accuracy classes A–C, the contribution of earthquake focal mechanisms to the overall statistical estimate $S_{H\max}$ reaches 85.8 %, and for accuracy classes A–E – 73.8 %. The second most important method is the borehole breakouts method [Heidbach et al., 2018]. It gives from 9.1 % for accuracy classes A–C to 14.7 % for accuracy classes A–E.

Estimates of $S_{H\max}$ are based on solving earthquake focal mechanisms and the seismic moment tensor (SMT). The seismic moment tensor is a mathematical description of the mechanisms of deformation of the geological environment near a seismic source. It characterizes the magnitude of the seismic event, the type of fracture (e. g., shear, tension), and the orientation of the fracture. The seismic moment tensor is a second-order tensor with nine independent components:

$$M = M_0 \begin{bmatrix} M_{11} & M_{12} & M_{13} \\ M_{21} & M_{22} & M_{23} \\ M_{31} & M_{32} & M_{33} \end{bmatrix} \quad (1)$$

where, M_0 is the seismic moment, M_{kj} are the components, which are pairs of forces consisting of opposing unit forces directed in the k – direction and separated by an infinitesimal distance in the j-direction.

To conserve angular momentum, the condition $M_{kj} = M_{jk}$ must be satisfied; therefore, the seismic moment tensor is symmetrical and has only six independent components. The simplest seismic moment tensor is the so-called double couple (DC), which describes the radiation pattern associated with pure sliding along the failure plane. In the case of the simplest point source, the displacement on the earth's surface at a station, can be represented as a linear combination of time-dependent elements of the seismic moment tensor $\mathrm{M_{kj}}(\boldsymbol{\xi}, t)$. These SMT elements have the same time dependence and are convolved with the derivative of the Green's function $\mathrm{G}_{skj}(\mathbf{x}, \boldsymbol{\xi}, t)$, relative to the spatial coordinate j (Bock, 2012)

$$\mathbf{u}_s(\mathbf{x}, t) = \mathrm{M}_{kj}(\boldsymbol{\xi}, t) * \mathrm{G}_{sk,j}(\mathbf{x}, \boldsymbol{\xi}, t) \quad (2)$$

where, $\mathbf{u}_s(\mathbf{x}, t) - s -$ component of soil displacement at point x and for time t; $\mathrm{M}_{kj}(\boldsymbol{\xi}, t)$ – 2nd order component, symmetric tensor of the seismic moment M; $\mathrm{G}_{sk,j}(\mathbf{x}, \boldsymbol{\xi}, t)$ – derivative of the Green's function with respect to the source coordinate ξ_j; $\mathbf{x}$ – vector characterizing the position of the station with coordinates x_1, x_2, x_3 for the north, east and downward direction; $\boldsymbol{\xi}$ is a vector characterizing the position of a point source with coordinates ξ_1, ξ_2, ξ_3.

The Green's function represents the impulse response of the medium between the source and the receiver. It takes into account various effects of wave propagation in a medium (energy loss due to reflection on seismic discontinuities, absorption and geometric divergence).

The seismic moment tensor $M_{kj}(\boldsymbol{\xi}, t)$ completely describes the forces acting in the source and their dependence on time. If we assume that all components $M_{kj}(\boldsymbol{\xi}, t)$ have the same time dependence $s(t)$, then equation (2) can be written as:

$$\mathbf{u}_s(\mathbf{x}, t) = M_{kj}[G_{sk,j}(\mathbf{x}, \boldsymbol{\xi}, t) \cdot s(t)] \qquad (3)$$

where, $s(t)$ is a function of the source action time or source time history.

$M_{kj}(\boldsymbol{\xi}, t)$ consists of nine pairs of equivalent mass forces. If the time function is expressed through the delta function ("needle" pulse), then $M_{kj}(\boldsymbol{\xi}, t) = M_{kj}(\boldsymbol{\xi}) \cdot \delta(t)$ and the right side of equation (3) is transformed to the form $M_{kj}(\boldsymbol{\xi}) \cdot G_{sk,j}(t)$.

Inversion of the seismic moment tensor allows estimation of fault plane parameters and the relationship between volumetric and non-volumetric strain in a seismic source [Knopoff & Randall, 1970]. It becomes possible to estimate the stress tensor based on the spatial orientation of the axes P (compression axis), T (tension axis) and B (zero axis), which are obtained by solving of earthquake focal mechanism. The B axis coincides with the intersection of two nodal planes. All three axes are orthogonal to each other and each is located at an angle of 90º to the other axes. The P and T axes are located at an angle of 45º to the nodal planes.

The components of the stress tensor characterize the stress state at a point in the medium. The forces acting on the surface of an infinitesimal cube can be decomposed into forces acting perpendicular (normal stress components) and parallel (tangential stress components) to the surface of an infinitesimal cube. The stressed state is described using 9 components of the stress tensor σ_{ij} (Fig. 1, *a*, formula (4)). Taking into account the symmetry of properties ($\sigma_{ij} = \sigma_{ji}$) under the condition $i \neq j$, only 6 components turn out to be independent.

$$\sigma_{ij} = \begin{pmatrix} \sigma_{11} & \sigma_{12} & \sigma_{13} \\ \sigma_{21} & \sigma_{22} & \sigma_{23} \\ \sigma_{31} & \sigma_{32} & \sigma_{33} \end{pmatrix} \qquad (4)$$

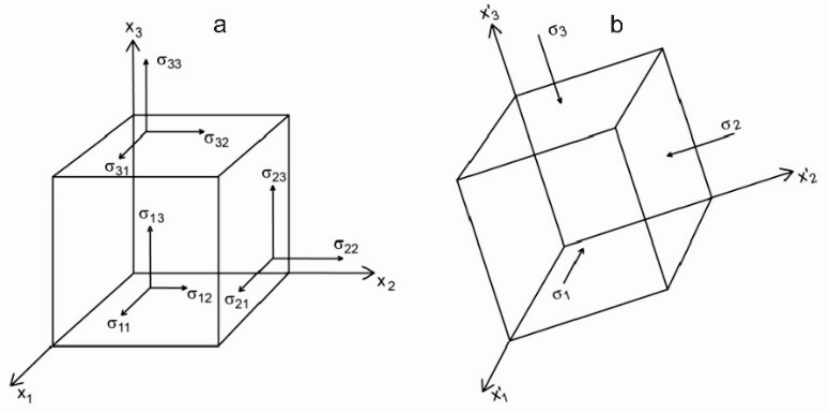

Fig. 1. Components of the stress tensor σ_{ij} (a) and principal stresses (b).

The stress state can always be transformed into such a coordinate system with the main axes (Fig. 1, *b*, formula (5)), in which only normal stresses remain, and shear stresses do not act, that is, equal to zero.

$$\sigma_{ij} = \begin{pmatrix} \sigma_1 & 0 & 0 \\ 0 & \sigma_2 & 0 \\ 0 & 0 & \sigma_3 \end{pmatrix} \qquad (5)$$

The components on the diagonal of the matrix (Fig. 1, *b*, formula (5)) represent the principal stresses, where σ_1 is the largest and σ_3 is the smallest. In this case, the condition $\sigma_1 \geq \sigma_2 \geq \sigma_3$ is satisfied. Other designations can be used to designate principal stresses ($S_1 \geq S_2 \geq S_3$). Vertical stress in the earth's crust can be estimated using the modified formula [Brown & Hoek, 1978]:

$$S_V = g\rho h, \qquad (6)$$

where g is acceleration, ρ is density, h is depth.

Vertical stress S_V is the principal stress at depth. The other two principal stresses of the stress tensor S_{Hmax} and S_{hmin} are projections of the principal stresses onto the horizontal plane. Thus, the stress state can be completely determined by four components (Fig. 2, formula (7)): the orientation of the vector $S_{H\max}$ and the scalar values of the main tectonic stresses S_V, $S_{H\max}$ and $S_{h\min}$

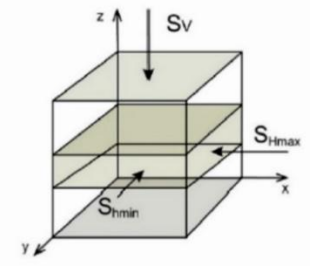

Fig. 2. Main tectonic stresses $S_{H\max}$, S_V, $S_{h\min}$.

$$S = \begin{pmatrix} S_V & 0 & 0 \\ 0 & S_{Hmax} & 0 \\ 0 & 0 & S_{hmin} \end{pmatrix} \quad (7)$$

In principle, there are three main tectonic stress regimes. Each tectonic stress regime is characterized by a certain ratio of principal stresses. For the case of normal faulting (NF) $S_V > S_{H\max} > S_{h\min}$, for the case of strike-slip faulting (SS) $S_{H\max} > S_V > S_{h\min}$ and for the case of trust faulting (TF) $S_{H\max} > S_{h\min} > S_V$. To create a tectonic stress map (Fig. 3), data for these three types of tectonic regimes, as well as data for an unidentified tectonic regime type U (unknown faulting), were used. In the latter case, only the azimuth $S_{H\max}$ was known [Slunga & Ahjos, 1986].

A web platform (https://www.world-stress-map.org/casmo) was used to map the vectors of the maximum horizontal stress $S_{H\max}$. Using the online tool CASMO, a stress map was created using the World Stress Map (WSM) database as well as our own user data. In particular, data on the $S_{H\max}$ directions for 4 earthquakes in Estonia from 2012 to 2018 were added to the WSM data.

Smoothing of the $S_{H\max}$ orientation was carried out on a regular grid applying a smoothing algorithm [Müller et al. 2003]. Direction vectors $S_{H\max}$ were calculated using a 0.5º grid with a search radius of 500 km, taking into account the quality of the data. With such a long-wavelength way of averaging, the influence of large-scale terrestrial structures is primarily considered, while the influence of local inhomogeneities is less noticeable. The data sample covered the depth range from 0 to 40 km. At the same time, in the depth range from 0 to 5 km, data on $S_{H\max}$ directions were obtained using all methods. For depths greater than 5 km, the estimation of $S_{H\max}$ directions was based on the earthquake focal mechanism [Heidbach et al., 2018].

Eight tectonic earthquakes occurred in the Eastern Baltic region for which the source mechanism could be determined (Fig. 3). Two Kaliningrad earthquakes of 2004 belong to accuracy class C, 4 Estonian earthquakes from 1976 to 2018 belong to class D and two Estonian earthquakes 2017.03.22 and 1980.01.19 belong to class E. Such a low accuracy class of these earthquakes is due to insufficiently large magnitudes, sparse seismic networks and large epicentral distances. The relatively high background level of seismic interference, geological conditions, and anthropogenic noise significantly reduced the ability to reliably determine the polarities of the first arrivals of *P*-waves for weak earthquakes [Soosalu et al., 2022].

Results and discussion

Parameters and map of earthquake focal mechanisms in the East Baltic region

Earthquake parameters listed in Table 1 include time of occurrence, epicenter coordinates, hypocenter depth, and magnitude. The earthquake focal mechanism parameters include strike, dip and rake for the two nodal planes, the azimuth of the maximum horizontal stress $S_{H\max}$ and the earthquake focal mechanism type (FM). Alternative earthquake focal mechanism type solutions evaluated by the authors are shown in ***Italics*** in the bottom line of the corresponding FM column (Table 1).

Table 1

Parameters and focal mechanisms of modern earthquakes in Eastern Baltic region

N	Date and time	Lat	Lon	*H*, km	*M*	*S*1	*D*1	*R*1	*S*2	*D*2	*R*2	$S_{H\max}$	FM	References
1	19761025 08:39	59.26	23.39	10	4.5	341	69	17	245	74	158	114	LLSS	Slunga, 1979
2	19800119 012453	58.71	24.01	10	2.3	–	–	–	–	–	–	100	UFM	Slunga & Ahjos,1986
3 a	20040921 11:05:03	54.86	19.98	15	4.6	29	86	23	298	67	175	161	RLLO	ZUR-RMT
3 b	20040921 11:05:03	55.03	20.21	18	4.5	204	64	–31	308	63	–151	166	NLLO	MED-RCMT
4 a	20040921 13:32:30	54.84	19.91	15	4.7	26	86	26	294	64	176	157	RLLO	ZUR-RMT
4 b	20040921 13:32:32	54.79	20.11	20.2	4.7	22	83	–5	113	85	–173	158	LLSS	GCMT
4 c	20040921 13:32:32	54.83	20.06	20.5	4.7	211	85	–8	302	82	–175	166	LLSS	MED-RCMT
4 d	20040921 13:32:31	54.81	20.09	3.0	5.6	119	73	–163	23	73	–17	160	RLSS	Nikulins & Malytskyy, 2021
5	20161112 02:49	58.29	26.19	4	1.8	348	80	39	251	52	168	114	LLSS ***RLLO***	Soosalu et al., 2022
6	20170322 03:00	59.34	24.36	4	1.2	155	66	33	50	61	152	102	***RLLO***	Soosalu et al., 2022
7	20170715 08:01	59.05	22.96	11.4	2.0	330	79	10	238	80	168	104	LLSS	Soosalu et al., 2022
8	20180304 01:21	58.93	23.69	3.5	1.7	151	70	4	60	87	160	107	LLSS	Soosalu et al., 2022

For each of the Kaliningrad earthquakes of September 21, 2004, several options for a focal mechanism solution are given from the most authoritative seismological agencies: *Swiss Seismological Service* (ZUR-RMT), *MedNet Regional Centroid – Moment Tensors* (MED-RCMT, INGV) and *Lamont Doherty Earth Observatory* (LDEO)), *Columbia University* (GCMT), as well as the authors' own estimates [Nikulins & Malytskyy, 2021]. Alternative results for the Kaliningrad earthquakes show that in the EBR for these earthquakes, even with maximum magnitudes, there is ambiguity in the assessment of some parameters (coordinates of the epicenter, hypocenter depth, magnitude). This is due to the different number of stations used by seismological agencies, the proximity of stations to the hypocenter, and the gap between stations. After 2015, earthquakes in EBR with small magnitudes were recorded thanks to the Estonian seismic network, which consists of 3 permanent and 7 temporary seismic stations. The stations are mainly located in northern Estonia. This made it possible to obtain data of satisfactory quality for studying earthquakes focal mechanisms in EstoniaComments: H – focal depth, M – magnitude, S1, D1, R1, S2, D2, R2 – strike, dip, rake for 1 and 2 nodal planes, respectively, FM – focal mechanism, $S_{H\max}$ – azimuth of maximum horizontal stress, LLSS – left-lateral strike-slip, RLLO – reverse left-lateral oblique, NLLO – normal left-lateral oblique, RLSS – right-lateral strike-slip, UFM – unknown focal mechanism, ZUR-RMT – *Swiss Seismological Service*, MED-RCMT – *MedNet Regional Centroid - Moment Tensors* (INGV), GCMT – *Lamont Doherty Earth Observatory* (LDEO), *Columbia University*.

Solutions to the earthquake focal mechanisms (Fig. 3) are given for the lower hemisphere and for projecttion – with an equal area. The earthquake focal mechanisms of EBR have a predominant type of movement: reverse and strike-slip. The mechanism of earthquake No. 5 by the Lake *Võrtsjärv*, in Estonia 2016/11/12, according to the primary source of information [Soosalu et al., 2022], is an oblique strike-slip. An alternative type of focal mechanism for this earthquake, assessed by the authors of the publication, is reverse left-lateral oblique. The mechanism of the earthquake No 6 in Estonia 2017/03/22 in the original source [Soosalu et al., 2022] was not determined due to the small magnitude (M = 1.2) and only two clear polarities. The authors rated the mechanism of this earthquake as reverse left-lateral oblique.

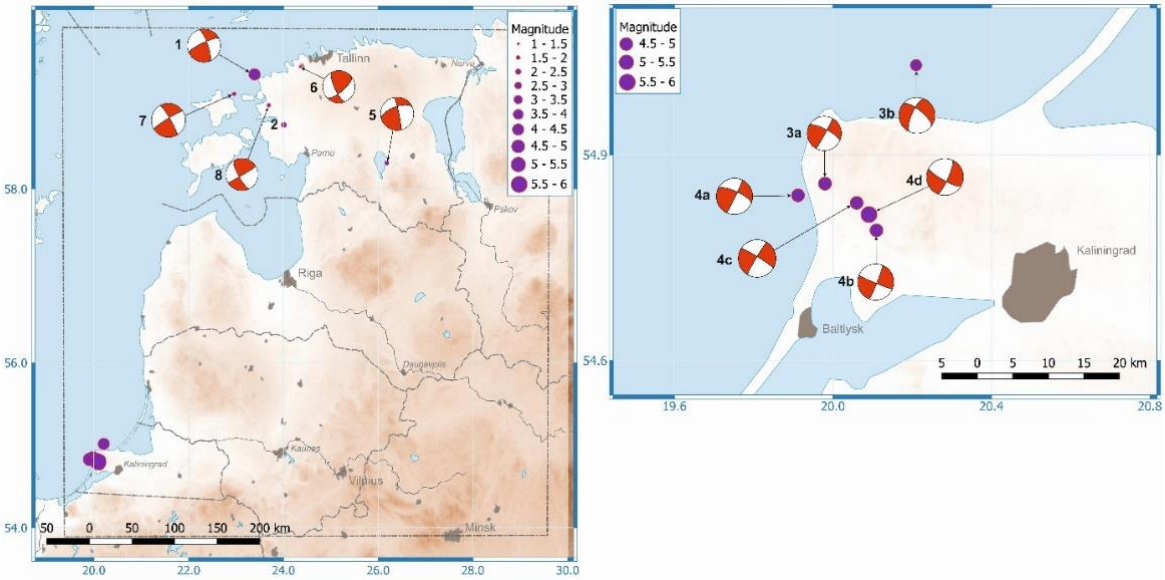

Fig. 3. Maps of earthquake sources of 1976–2018 in the East Baltic region for the instrumental period.

According to geological, seismic and drilling data, tectonic faults on the territory of Latvia are considered mainly as faults with an almost vertical fault plane. In this form, these faults are present in almost all geological sections. Only in one case Olaine – Incukalns fault), the tectonic regime is characterized as a reverse fault by using seismic methods and well drilling, [Brangulis, & Kanevs, 2002].

The map in Fig. 4 shows three profiles intersecting the EBR. The longest southwest-northeast profile (21 red dots on 1-st profile) passes through the epicenters of the 2004 Kaliningrad earthquakes and the 1976 Osmussaar earthquake. Estimates of the orientation of $S_{H\max}$ in this direction are the most reliable. Starting from point No 6, the $S_{H\max}$ azimuth decreases.

The northwest-southeast profile (8 blue dots on 2-nd profile) crosses the Baltic Sea, passes through northern Kurzeme, Riga and extends in the direction of the Plavinu hydroelectric station (HPS), which is located in unfavorable geodynamic conditions [Nikulins, 2019]. These conditions are caused by two tectonic faults (Aizkraukle and Piebalga), which are located near the hydroelectric power station, forming a graben-like structure. In the area of the Plavinu HPS there are a number of unfavorable geodynamic, geological, hydrogeological and other factors. Therefore, estimation and knowledge of the $S_{H\max}$ parameters in this area is of great practical importance.

The profile of orientation $S_{H\max}$ in the direction southwest – northeast (12 green points on 3-rd profile) coincides with the Deep Seismic Sounding (DSS) profile of 1986 in the direction Sovetsk – Riga – Kohtla – Jarve [Ankudinov et al., 1991]. This profile allows one to correlate the change in orientation of $S_{H\max}$ with the deep structure.

Fig. 4 shows the epicenter of the 1980/01/19 01:24:52.8 earthquake [Slunga & Ahjos, 1986] with an unknown tectonic mode "U", near points 11 and 12 (1 profile). The earthquake had a magnitude of 2.3 ML and was included in the WSM database. Although the focal mechanism of this earthquake is unknown, the horizontal stress direction was estimated to be 100º for it. The epicenter of this earthquake is shown in Fig. 3. Rotation of the vectors $S_{H\max}$ occurs inside the EBR. In north of Estonia the $S_{H\max}$ azimuth is 105–110º, in Latvia it increases to 115–150º, and it reaches 160–180º in Lithuania.

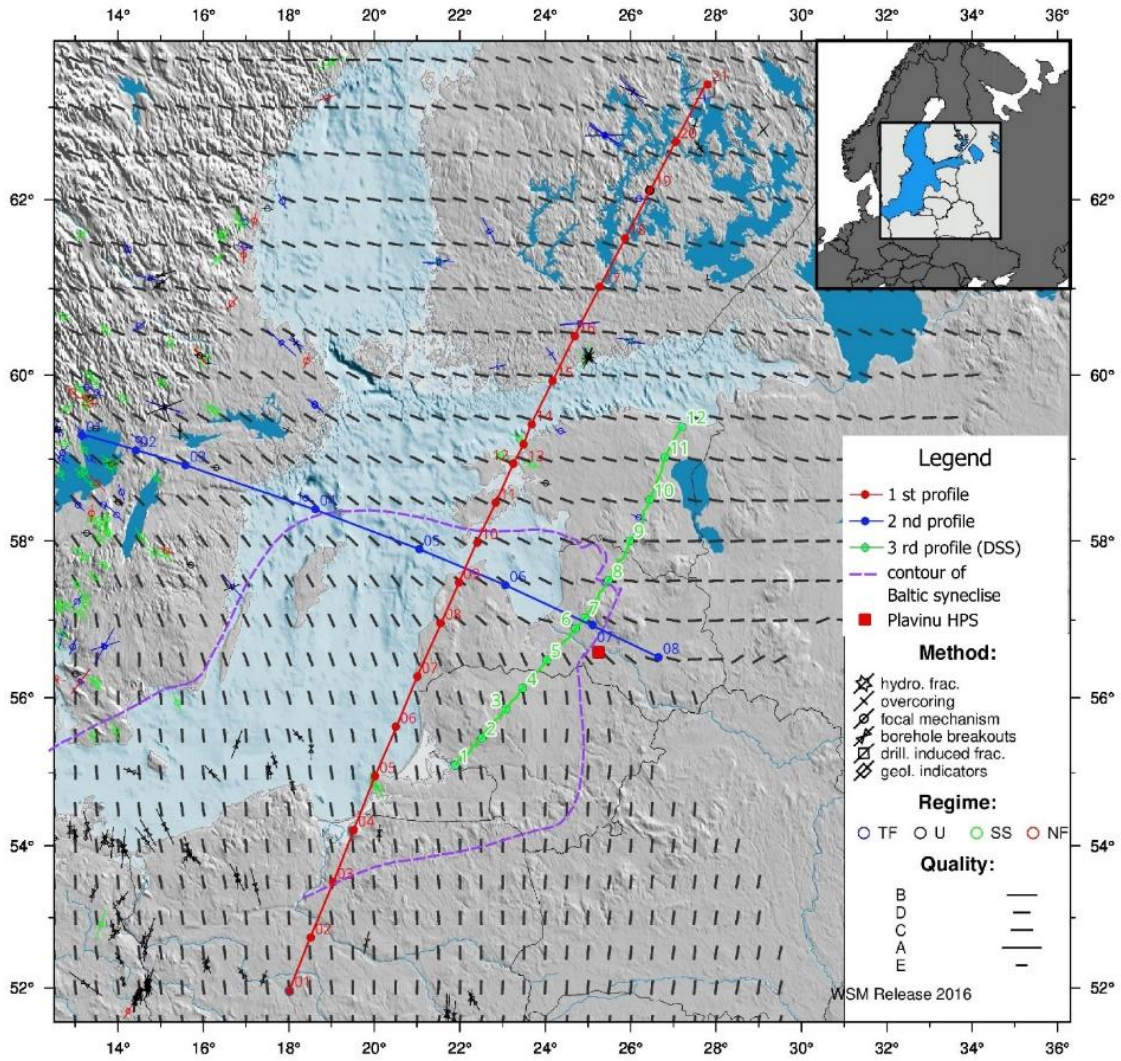

Fig. 4. Map of maximum horizontal stresses $S_{H\max}$ vectors in the Baltic region:
Comments: red color – profile 1 and points on profile 1, blue color – profile 2 and points on profile 2, green color – 1986 DSS profile and points on the profile 3, the purple dotted line shows the outline of the Baltic syneclise.

Assessment of the influence of sedimentary cover and deep geological structure on the orientation of $S_{H\max}$ vector.

To understand the reason for the rotation of the $S_{H\max}$ vectors, the possible influence of the sedimentary cover and the deep structure of the earth's crust was analyzed.

Stress fields in sedimentary basins result from a complex combination of multiple factors operating at multiple scales, including far-field forces (e. g., forces acting at tectonic plate boundaries), basin geometry (e. g., the shape of deltaic wedges), geological structures (e. g., diapirs, faults), mechanical contrasts (e. g. evaporites, overpressured shales, detachment zones), topography and deglaciation [Tingay, 2009].

Analysis of the distribution of $S_{H\max}$ vectors shows that within the Baltic syneclise (Fig. 4) this direction changes from 120º in the north part (point 10 on 1-st profile, Fig. 5) to 170–175º in the south part (point 3 on 1-st profile, Fig. 5). The thickness of the sedimentary cover also changes in the same direction. Therefore, for example, if in the northern part of the Baltic syneclise the thickness of the sedimentary cover is 0.6–0.7 km, then in the southern part it increases to 2.7 km [Paskevicius, 1997]. According to the DSS profile Sovetsk – Riga – Kohtla-Jarve, the thickness of the sedimentary cover varies from 2.1 to 0.25 km [Ozolinya & Kovrigin, 1986]. Thus, within the Baltic syneclise, there is no obvious dependence of the $S_{H\max}$ azimuths on the thickness of the sedimentary cover. Only in certain parts of the syneclise one can note a decrease in azimuths $S_{H\max}$ and a decrease in the thickness of the sedimentary cover in the direction from south to north (Fig. 5). For example, this can be seen on profile 1 from point 6 to point 10 or on profile 3 from point 4 to point 8 (Fig. 5) .

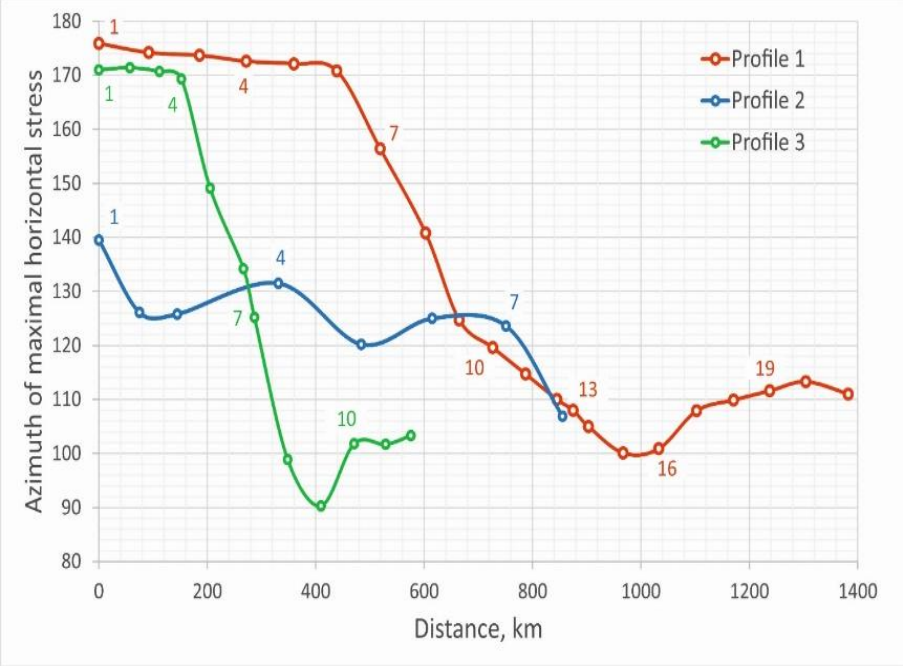

Fig. 5. Profiles of changes in the azimuth of the maximum horizontal stress $S_{H\max}$ in the Baltic region.

The change in azimuths $S_{H\max}$ was analyzed along the deep seismic sounding profile Sovetsk – Riga – Kohtla-Jarve (Fig. 6). The following characteristic features can be distinguished.

Azimuth $S_{H\max}$ begins to decrease after point 4 on profile 3 (Fig. 5 and 6). In the area between points 4 and 5 (this corresponds to a distance of 150–200 km from the beginning of the profile), the DSS profile crosses the Taurage-Ogre deep tectonic fault. The depth of the fault is almost 60 km. This fault forms a step at the Moho boundary M_1 and the intramantle boundary M_2. Other deep faults (Fig. 6) do not have the same significant effect on the change in azimuth $S_{H\max}$. A sharp shift of the Moho boundary does not always correspond to a change in azimuth $S_{H\max}$. For example, despite the sharp shift of the M_1 boundary, at DSS profile points 280–320 km, then the decrease in azimuth $S_{H\max}$ occurs smoothly and gradually. The minimum azimuth value $S_{H\max}$ 90º is achieved at DSS profile point 410 km. The azimuth $S_{H\max}$ slightly increases to 100–103º after the Paldiski-Pskov deep fault near DSS profile point 460 km. Thus, the influence of a deep fault on a significant change in the azimuth $S_{H\max}$ was only noted in one case.

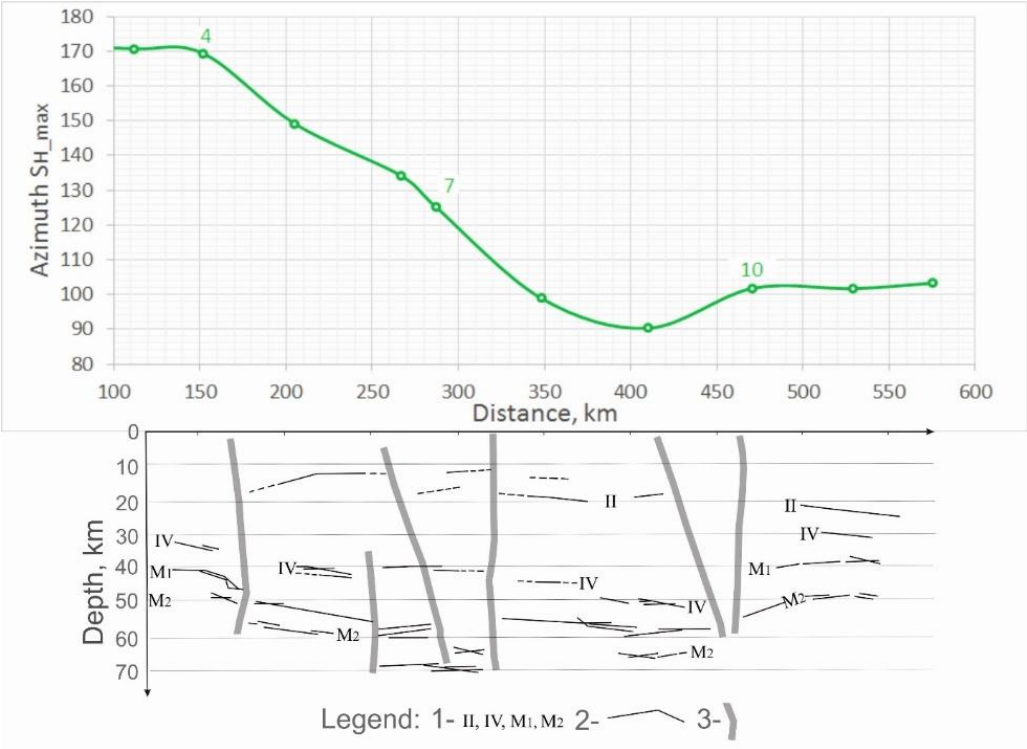

Fig. 6. Deep structure of the earth's crust along the DSS profile Sovetsk – Riga – Kohtla-Jarve and the corresponding change of azimuth maximum horizontal stress $S_{H\max}$ along the profile.Legend:

1 – indices of the main interfaces in the earth's crust and upper mantle;
2 – main interfaces in the earth's crust and upper mantle; 3 – deep tectonic fault zones.

Estimation of the influence of the gravitational field on the orientation of the $S_{H\max}$ vectors

According to some studies, gravity anomalies can be used for estimating the magnitude of deviatoric stress in the earth's crust and upper mantle, as a measure of the Earth's deviation from hydrostatic equilibrium [McNutt, 1980].

To clarify the relationship between the directions of $S_{H\max}$ and the gravitational field, we investigated the connection of the gravitational field along the Sovetsk – Riga – Kohtla-Jarve DSS profile with $S_{H\max}$ azimuth. On this profile, gravity anomalies from various parts of the earth's crust were assessed. The earth's crust includes the following layers: 1) sedimentary layer with a thickness of 0.25 to 2.1 km; 2) the upper part of the crystalline basement; 3) the lower part of the crystalline basement; 4) granite-metamorphic layer up to the conventional boundary "II" with a thickness of 10–25 km; 5) diorite-granulite layer (granite) up to the "IV" boundary, i. e. to the Conrad discontinuity, with a thickness of 17–24 km; 6) mafic-granulite layer (basalt) 8–24 km thick to the Moho boundary "M_1"; 7) crust-mantle layer with a thickness of 5–10 km, between the boundary "M_1" and the intra-mantle boundary "M_2".

The gravity parameters were based on studies to summarize the physical properties of Latvian rocks [Ozolinya & Kovrigin, 1986]. The density model of the sedimentary cover was based on the correlation between the average density and the average velocity and thickness of the sedimentary cover. This dependence with a correlation coefficient of 0.82 has the formula:

$$\sigma_{ave} = 1.964 - 0.013H + 0.169V_{ave}, \qquad (8)$$

where σ_{ave} – average density of sedimentary cover, G/cm^3; H – sedimentary cover thickness, km; V_{ave} – average velocity in sedimentary cover, km/sec.

The gravitational influence of individual layers of the earth's crust is assessed. The following notations were used for the parameters of the gravitational influence of individual layers of the earth's crust: Δg_{OBS} – observed gravitational field; Δg_{LI} – the lateral influence of the surrounding upper part of the earth's crust in the band ±90 km from the DSS profile and to a depth of 10 km; $\Delta g_{DF} = \Delta g_{OBS} - \Delta g_{LI}$; Vz_{SC} – gravitational effect of the sedimentary cover; $\Delta g' = \Delta g_{DF} - Vz_{SC}$; Vz_{UPCB} – gravitational effect of the upper part of the crystalline basement; $\Delta g'' = \Delta g' - Vz_{UPCB}$; $\Delta g''_{ave} = \Delta g' - Vz_{UPCB}$, gravitational field $\Delta g''$ averaged over a sliding interval of 40 km; Vz_{LPCB} –

gravitational effect of the lower part of the crystalline basement; $\Delta g''' = \Delta g''_{ave} - Vz_{LPCB}$; Vz_{IV} – gravitational effect of the layer up to the IV boundary; Vz_{M1} – gravitational effect of the layer up to the M_1 boundary; Vz_{M2} – gravitational effect of the layer up to the M_2 boundary; ΣVz – the sum of all gravitational effects; $\Delta g_{OBS} - \Sigma V_Z$ – the difference between the observed gravitational field Δg_{OBS} and the sum of all gravitational effects ΣV_Z.

The gravitational effect of the sedimentary cover is mainly due to changes in the thickness of the sedimentary cover and, to a lesser extent, to changes in density. This effect decreases along the DSS profile from north to south (from 590 km to 70 km) from –5 mGal to –27 mGal. The lateral influence of the surrounding upper crust is negligible. It varies from a minimum value of 0.0 mGal (70 km) to a maximum value of 3.2 mGal (510 km). The gravitational field $\Delta g''$ is complicated by small local anomalies (Fig. 7). It is "free" from the influence of deep layers of the earth's crust. The averaged gravitational field $\Delta g''_{ave}$ does not have these shortcomings.

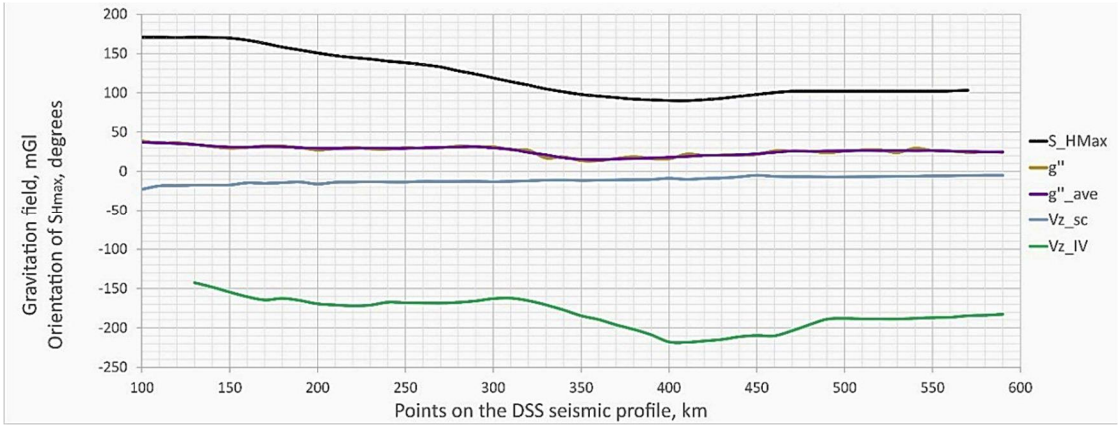

Fig. 7. The relationship between the direction of $S_{H\max}$ and some effects of the gravitational field along the profile of the DSS *Sovetsk – Riga – Kohtla-Jarve* Legend: $S_{H\max}$ – maximal horizontal stress direction, $\Delta g'' = \Delta g_{OBS} - (\Delta g_{LI} + Vz_{SC} + Vz_{UPCB})$; $\Delta g''_{ave}$ – gravitational field $\Delta g''$ averaged over a sliding interval of 40 km; Vz_{SC} – gravitational effect of the sedimentary cover; Vz_{IV} – gravitational effect of the layer up to the IV boundary (Fig. 6).

The highest correlation coefficient (negative) r = –0.85 is observed between the direction $S_{H\max}$ and the gravitational effect Vz_{SC} of the sedimentary cover. With a negative correlation, an increase in one variable corresponds to a decrease in another variable.

However, this influence was stated only on part of the Baltic syneclise, i. e. sedimentary cover. For other areas of the sedimentary cover of the EBR, such a relationship was not studied due to the lack of sufficient data.

Table 2

Correlation coefficients between the azimuth $S_{H\max}$ and the gravitational influence of individual layers of the earth's crust section along the Sovetsk – Riga – Kohtla-Jarve DSS profile

	Δg_{obs}	Δg_{DF}	Vz_{SC}	$\Delta g'$	Vz_{UF}	$\Delta g''$	$\Delta g''_{ave}$	Vz_{LF}
$S_{H\max}$	−0.54	−0.55	−0.85	−0.17	−0.66	0.80	0.84	−0.51
	$\Delta g'''$	Vz_{IV}	Vz_{M1}	Vz_{M2}	ΣVz	$\Delta g_{obs} - \Sigma Vz$		
$S_{H\max}$	0.71	0.83	−0.027	0.154	0.199	−0.80		

High positive correlation coefficients (from 0.84, 0.83 and 0.80) are also observed with the gravitational field $\Delta g''_{ave}$, averaged in a sliding windows of 40 km, with the gravitational effect Vz_{IV} of the layer up to boundary IV and with the gravitational effects $\Delta g'' = = \Delta g_{OBS} - (\Delta g_{LI} + Vz_{SC} + Vz_{UPCB})$ and the differrence between the observed gravitational field Δg_{OBS} and the sum of all gravitational effects ΣV_Z ($\Delta g_{OBS} - \Sigma V_Z$).

Conclusions

Earthquake focal mechanisms in the East Baltic region were generalized, the predominant mechanisms being strike-slip and reverse. In some cases, these mechanisms had an oblique component.

Within the Baltic syneclise, one can note a decrease in azimuths $S_{H\max}$ and a decrease in the thickness of the sedimentary cover in the direction from south to north.

The direction of the maximum horizontal stresses $S_{H\max}$ changes from north (Estonia) to south (Kaliningrad district of the Russian Federation) from 102º–114º to 157º–166º. A sharp change in the direction of $S_{H\max}$ was noted in the area of only one deep fault. In other cases, such a sharp change of $S_{H\max}$ direction was not observed. The correlation of the $S_{H\max}$ direction with the gravitational influence of individual layers of the deep section of the earth's crust showed the ambiguous influence of the sedimentary cover.

A map of $S_{H\max}$ vectors in the Baltic region was constructed based on the direction of the maximum horizontal stresses $S_{H\max}$ in the region of southern Scandinavia and Eastern Europe, taken from the WSM database and additional data for the territory of Estonia. Due to the limited data for the Eastern Baltic region on the mechanisms of earthquake foci, the studies made it possible to obtain only a generalized map of the $S_{H\max}$ direction. Nevertheless, these results are important for more effective assessment of geodynamic conditions in areas of important engineering structures (nuclear power plants, hydroelectric power plants, underground storage facilities for radioactive materials and hydrocarbons).

The full stress tensor will allow modeling the geodynamic situation in the area of important engineering structures and estimating the parameters of movement and deformation, which will be shown in future publications.

References

Avotinya, I. Ya., Boborykin, A. M. et al. (1988). Catalog of historical earthquakes in Belarus and the Baltic states. Seismological bulletin of seismic stations “Minsk” (Pleschenitsy) and “Naroch” for 1984, 126–137 (in Russian).

Ankudinov, S. A., Brio, H. S., & Sadov, A. S. (1991). The deep structure of the earth's crust on the territory of the Baltic republics according to seismic data from the Deep Seismic Sounding. *Belarusian Seismological Bulletin*, 1, 111–117 (in Russian).

Boborykin, A. M., Garetsky, R. G., Emelyanov, A. P., Sildvee, H. H., & Suveizdis, P. I. (1993). Earthquakes of Belarus and the Baltic States. *Current state of seismic observations and their generalizations (Methodological works of ESSN)*, 4, 29–39.

Bock, G. (2012). Source parameters and moment-tensor solution. GeoForschungZentrum Potsdam, Germany. 14 p., https://doi.org/10.2312/GFZ.NMSOP-2_IS_3.8

Brangulis, A., & Kanevs, S. (2002). Latvijas tektonika. Valsts geologijas dienests, 50 p.

Brown, E. T, & Hoek, E. (1978). Trends in relationships between measured in situ stresses and depth. Int. *J. Rock Mech. Min. Sci. Geomech. Abstr.,* 15, 211–215. https://www.rocscience.com/assets/resources/learning/hoek/Trends-in-Relationship-between-Measured-In-Situ-Stresses-and-Depth-1978.pdf

Doss, B. (1910). Die historisch beglaubigten Einsturzbeben und seismisch-akustischen Phänomene der russischen Ostseeprovinzen. *Beiträge zur Geophysik. Leipzig*, X. Band, pp. 1–124.

Gregersen, S., Wiejacz, P., Debski, W., Domanski, B., Assinovskaya, B., Guterh, B., Mantyniemi, P., Nikulin, V. G., Pacesa, A., Puura, V., Aronov, A. G., Aronova, T. I., Grunthal, G.,Husebye, E. S., & Sliaupa, S. (2007). The exceptional earthquakes in Kaliningrad district, Russia on September 21, 2004. *Physics of the Earth Planetary Interiors,* 164, 63−74. https://doi.org/10.1016/j.pepi.2007.06.005

Heidbach, O., M. Rajabi, K. Reiter, M. O. Ziegler, WSM Team (2016). World Stress Map Database Release 2016. *GFZ Data Services*, https://doi.org/10.5880/WSM.2016.001

Heidbach, O., M. Rajabi, X. Cui, K. Fuchs, B. Müller, J. Reinecker, K. Reiter, M. Tingay, F. Wenzel, F. Xie, M. O. Ziegler, M.-L. Zoback, and M. D. Zoback (2018). The World Stress Map database release 2016: Crustal stress pattern across scales. *Tectonophysics*, 744, 484–498. https://doi.org/10.1016/j.tecto.2018.07.007

Hergert, T, & Heidbach, O. (2011). Geomechanical model of the Marmara Sea region – II. 3D contemporary background stress field. *Geophysical Journal International, 185(3),*1090–1102. https://doi.org/10.1111/j.1365-246X.2011.04992.x

Knopoff, L., & Randall, M. J. (1970). The compensated linear-vector dipole. A possible mechanism for deep earthquakes, *Journal of Geophysical Research, 75*(26), 4957–4963. https://doi.org/10.1029/JB075i026p04957

McNutt, M. (1980). Implications of Regional Gravity for State of Stress in the Earth’s Crust and Upper Mantle. *Journal of Geophysical Research*, 85 (B11), 6377–6396. https://doi.org/10.1029/JB085iB11p06377

Müller, B, Wehrle, V, Hettel, S, Sperne,r B, & Fuchs, F. (2003). A new method for smoothing oriented data and its application to stress data. *In: M Ameen (ed) Fracture and in situ stress characterization of hydrocarbon reservoirs. Special Publication: Geological Society, London, 209*(1), 107–126. https://doi.org/10.1144/GSL.SP.2003.209.01.11

Nikonov, A. A., & Sildvee, H. (1991). Historical earthquakes in Estonia and their seismotectonic position. *Geophysica*, *27*(1–2), 79–93. https://www.geophysica.fi/pdf/geophysica_1991_27_1-2_079_nikonov.pdf

Nikulins, V. (2019). Geodynamic Hazard Factors of Latvia: Experimental Data and Computational Analysis. *Baltic Journal of Modern Computing*, *7* (1), 151–170. https://doi.org/10.22364/bjmc.2019.7.1.11

Nikulins, V., Malytskyy D. (2021). Focal mechanism of the Kaliningrad earthquake of 21 September 2004 based on waveform inversion using a limited number of stations. *Baltica*, *34*(1), 95–107. https://doi.org/10.5200/baltica.2021.1.8

Ozolinya, N. K., & Kovrigin, V. P. (1986). Report on the topic "Generalization of the physical properties of rocks on the territory of the Latvian SSR" for 1984–1986. *Geology Department of the Latvian SSR*, KGE, Vol. 1, 144 p.

Paskevicius J. (1997). The Geology of the Baltic Republics. Vilnius, 387 p.

Slunga, R. S. (1979). Source mechanism of a Baltic earthquake inferred from surface wave recordings. *Bulletin of the Seismological Society of America*, *69*(6), 1931–1964. https://doi.org/10.1785/BSSA0690061931

Slunga, R., & Ahjos, T. (1986). Fault mechanisms of Finnish earthquakes, crustal stress and faults. *Geophysica*, *22*(1–2), 1–13. https://archive.geophysica.fi/pdf/geophysica_1986_22_1-2_001_slunga.pdf

Soosalu, H., Uski, M., Komminaho, K., Veski, A. (2022). Recent Intraplate Seismicity in Estonia, East European Platform. *Seismological Research Letters*, *93*(3), 1800–1811. https://doi.org/10.1785/0220210277

Tingay M. (2009). State and Origin of Present-Day Stress Field in Sedimentary Basin. *ASEG Extended Abstracts*, 1, 1–10. https://doi.org/10.1071/ASEG 2009ab037

Валерій НІКУЛІНС, Дмитро МАЛИЦЬКИЙ[2]

[1] SIA Geo Consultants, Olivu iela 9, Riga, LV-1004, Латвія, e-mail: seismolat@gmail.com, https://orcid.org/0000-0003-4489-8708

[2] Карпатське відділення Інституту геофізики ім. Субботіна Національної академії наук України, e-mail: dmalytskyy@gmail.com, https://orcid.org/0000-0002-9156-739X

МОДЕЛЬ ТЕКТОНІЧНИХ НАПРУЖЕНЬ У СХІДНО-БАЛТІЙСЬКОМУ РЕГІОНІ

Систематизовано параметри та механізми вогнищ сучасних землетрусів у регіоні Східної Балтії. Переважають такі типи механізмів вогнищ материкових землетрусів, як ***Strike-slip і Reverse***. Створено узагальнену карту орієнтації максимальних горизонтальних напружень у Східно-Балтійському регіоні та на прилеглих територіях. Щоб створити цю карту, ми використали базу даних World Stress Map і додали напрямки максимальних горизонтальних напружень в Естонії. Напрямок максимальних горизонтальних напружень змінюється із півночі (Естонія) на південь (Калінінградська область РФ) від 102º–114º до 157º–166º. Ми дослідили, як глибинна геологічна структура та гравітаційні сили в різних частинах земної кори впливають на напрямок максимальних горизонтальних напружень. З'ясовано, що напрямок максимального горизонтального напруження змінювався під час перетину лише одного глибокого тектонічного розлому. Виявлено високі значення кореляції напрямку максимального горизонтального напруження із гравітаційним впливом осадового чохла (від'ємну кореляцію), усередненим різницевим гравітаційним полем і гравітаційним впливом шару земної кори до границі *Конрада*.

Ключові слова: механізм вогнища землетрусу, тензор сейсмічного моменту, параметри вогнища землетрусу, головні напруження, максимальне горизонтальне напруження, Східно-Балтійський регіон, World Stress Map.

Received 02.04.2024